Article

Spatiotemporal Analysis of Urban Carbon Metabolism and Its Response to Land Use Change: A Case Study of Beijing, China

Yingjie Hu [1], Jin Sun [2] and Ji Zheng [3,*

[1] College of City Construction, Jiangxi Normal University, Nanchang 330022, China
[2] College of Surveying and Geo-Informatics, North China University of Water Resources and Electric Power, Zhengzhou 450000, China
[3] Department of Urban Planning and Design, The University of Hong Kong, Hong Kong 999077, China
[*] Correspondence: zhengji@hku.hk

Abstract: Analyzing the spatial pattern of urban carbon metabolism could provide insights into spatial adjustments to mitigate the greenhouse effect. Using CASA and empirical coefficients, we quantitatively analyzed and mapped the spatial pattern of the urban carbon metabolism of Beijing and its response to land use change from 2000 to 2020. The results showed that the carbon emission rate of Beijing increased in the first decade and decreased in the next, while the carbon sequestration rate kept rising over the past two decades. The net carbon emission rate of Beijing averaged 1284.52×10^7 kg C yr^{-1}, indicating that the city functioned as a net carbon source throughout the study period. The most harmful carbon transitions were always sourced from the southeastern suburban area, where the natural components were converted to artificial components, while beneficial carbon transitions were in the urban central area, where the artificial component with a higher carbon emission density was converted to the other types of artificial components with relatively a lower carbon emission density, and the northwestern mountainous areas, where land use types transferred out of and into the forest or grass. The spatiotemporal change in urban carbon metabolism was highly correlated with the land use transition, and the land use change from cultivated land to industrial land accounted for 34.87% of the harmful carbon transitions. These results of key carbon flows and hotspots provide insights for policymaking in the effective management of reducing carbon emissions and enhancing carbon sequestration.

Keywords: urban carbon metabolism; spatial pattern; low-carbon development

1. Introduction

Urban areas are the primary contributor to global carbon emissions and have been prioritized in the mitigation agenda [1]. Accounting for only 2% of the world's total land area, urban areas support 55% of the world's population and contribute nearly 75% of global energy consumption-related greenhouse gas (GHG) emissions [2,3]. Land use and cover change (LUCC), such as the replacement of vegetated surfaces with built-up land, result in almost one-third of urban carbon emissions [4]. As the present largest emitter in the world, China has experienced a remarkable urbanization process since its Reform and Opening Up [5]. The ongoing rapid urbanization process has inevitably profoundly influenced land use patterns, which are generally characterized by the transition from natural lands (e.g., forest land and grassland) to artificial lands (e.g., residential and industrial lands), and these strongly affect the quantitative and spatial features of urban carbon emission and sequestration [6,7]. The LUCC-related carbon emissions of China accumulated to almost 1.45 Pg from 1990 to 2010, and 45% of those resulted from urban expansion [7,8]. It is a great challenge for China to mitigate carbon emissions and meet its commitment to peak carbon emissions around 2030 and achieve carbon neutrality by 2060 [9] while urbanization in China is rapidly proceeding. From the perspective of low-carbon regulation,

cities are the key areas for implementing emission reduction measures in China [10]. Thus, an understanding of the spatial and temporal urban carbon metabolism characteristics is of great significance for formulating practical and reasonable mitigation policies from a land-based perspective.

Urban carbon metabolism mostly refers to carbon flows, including both emissions and sequestration, between the different components of the urban system [11,12]. Quantifying urban carbon emissions and the sequestration of both natural and artificial components is an important basis for comprehensively assessing urban carbon metabolism. Substantial efforts have been dedicated to exploring carbon emissions [13,14] and sequestration changes [10,15,16] based on LUCC changes [11–14]. Both carbon emissions and sequestration show significant regional disparities. Carbon sequestration is correlated with land cover types in natural systems and environmental conditions [17–19]. Carbon emissions are related to the quantity and structure of energy consumption by transportation and industry [20–22], urban and rural households [23–25], and agricultural activities [26,27]. In addition to showing quantity differences, previous research has also shown that the spatial pattern of carbon sinks and sources differs among cities and within cities [28,29]. The spatial variation in the carbon budget between urban and peri-urban areas is significant as well. Hutyra et al. [30] took the lowland Seattle Statistical Metropolitan Area (MSA) region as a case study and explored the spatial variation in carbon consequences of LUCC as a function of the distance from the city center. Therefore, understanding the past patterns and carbon consequences of LUCC is not only important for diverse and global knowledge on urban carbon studies but also critical for informing suitable land development strategies for local cities.

Many researchers recognize that a complete overview of urban carbon flow processes should include the artificial components of carbon emissions and sequestration and the changes in these components caused by LUCC. Substantial efforts have been dedicated to quantifying LUCC-related carbon flows, aiming to explore carbon regulation strategies using land use management [31–33]. Numerous existing studies have summarized only one aspect, namely, they have focused on either the carbon emissions of different economic activities and their interactions [18,34] or the carbon sequestration of the city's natural processes [35,36]. More recently, some scholars have studied carbon metabolism considering both aspects since urban carbon metabolism follows the law of conservation of matter, and carbon emission studies should also consider the flows and changes caused by increasing or decreasing carbon storage to give a complete description of urban carbon flows [37–39]. Zhang et al. [40] analyzed carbon transitions between the artificial and natural components of Beijing, analyzed the rates and spatial patterns of carbon emissions and sequestration, and quantified carbon flows using an LUCC matrix from 1990 to 2008. Xia et al. [41] assessed the carbon transitions (carbon flows) caused by land use changes in Hangzhou through an assessment of carbon emissions and sequestration from 1995 to 2015. The above studies have quantified the impacts of LUCC on carbon flow variability and revealed the key carbon flow paths during different periods. The decrease in net carbon emissions was mostly attributed to the decline in emission intensity of certain types of construction land, such as transportation and industrial land, while the increase in net carbon sequestration was mainly attributed to the recovery of green space [41,42].

However, the above studies focused on carbon flows in the land use transitions but ignored the carbon change in the unconverted land use type (e.g., the decline in the carbon emissions of unconverted transportation and industrial land with declining emission intensity, and the increase in the carbon sequestration of unconverted recovering natural space). Since urban carbon sequestration is affected by many additional factors, including vegetation structure, climate change, etc. [43], the carbon sequestration of the unconverted urban component is also temporally dynamic and spatially heterogeneous. The spatial heterogeneity of the carbon sequestration of the same land use type and the temporal dynamic of the unconverted land use type have not been well revealed because most of the above studies applied empirical coefficients to evaluate carbon emissions and sequestration

on the basis of the land use type. Among the methods used to evaluate carbon fluxes, approaches based on remote sensing are relatively convenient and economical for data collection but are sensitive to the resolution and quality of the raw remote sensing data [44]. As a conjunction of remote sensing and GIS technologies and a large-scale land database, the Carnegie–Ames–Stanford Approach (CASA) model, which calculates regional carbon storage and its spatial distribution on the basis of the principle of effective radiation absorption of light energy by vegetation [45], has commonly been used to evaluate carbon storage in ecosystems with a large scale [46,47].

As the capital of China, Beijing is one of the most developed cities and has the highest urbanization level in the world. The urban population in Beijing grew from about 5.21 million (57.62%) in 1980 to 1916.6 million (87.54%) in 2020 [48]. The unprecedented urbanization resulted in significant changes in land use and a dramatic increase in carbon emissions, leading to a tough challenge for carbon mitigation. Consequently, this study used Beijing as the target case and analyzed the quantity and spatial pattern of urban carbon metabolism with land use change by evaluating carbon emissions and carbon sequestration. Specifically, we not only examined the carbon flows caused by land use change using a land-use change (transfer) matrix from 2000 to 2020 and divided these transitions into beneficial processes and harmful processes, but we also analyzed the carbon change of the unconverted land use type during four periods. The results provide empirical insights into how to make better urban planning and management decisions to achieve low-carbon city development in Beijing.

2. Materials and Methods

2.1. Study Area and Data Description

Beijing is a megacity with an area of 16,410.54 km^2 and an average elevation of 43.71 m located in the northwest of the North China Plain. The northwest of the city is dominated by mountains and hills, accounting for 62% of the area, while the central and southeastern areas are flat plains (Figure 1). During the past four decades, Beijing has experienced rapid industrial development and economic growth. From 1990 to 2020, the per-capita GDP of Beijing increased from CNY 4635 to 164,889 [48], and Beijing is currently ranking first among the major cities across the country. Along with rapid economic development and urbanization, Beijing is facing serious decarbonization challenges.

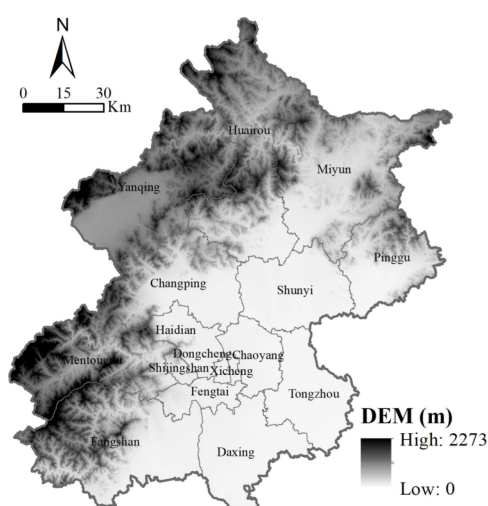**Figure 1.** Digital elevation model (DEM) of the study area of Beijing.

The data used in this study included land use type data, meteorological data, NDVI data used in carbon sequestration evaluation, agriculture data, energy and fuel consumption data used in carbon emission accounting, and other basic data. The land use type data for the years 2000, 2005, 2010, 2015, and 2020 were obtained from the Institute of Remote

Sensing Applications, Chinese Academy of China [49], generated from Landsat-TM/ETM and Landsat 8 images from the corresponding years [50,51]. The integrated discrimination accuracy for the various land use types reached 95% or above. The spatial resolution of this data was 100 m × 100 m. Depending on the category of land use type data, we choose the Tier 2 typology for construction land and used Tier 1 for the other land use types since this study focused on urban carbon metabolism and its relationship with urban land use change, which was also applied widely in the existing research [28,52]. Table 1 illustrates the eight components contained in the urban metabolism system: cultivated land (C), forest (F), grassland (G), water (W), urban land (U), rural land (R), transportation and industrial land (T), and bare land (B). Bare land is unused land with little or no vegetation or signs of human activity and is thus assumed to have no carbon flow since carbon sequestration and emissions are negligible. The Normalized Difference Vegetation Index (NDVI) data used to evaluate the carbon sequestration in the selected years were derived from the Terra Moderate Resolution Imaging Spectroradiometer (MODIS) Vegetation Indices (MOD13Q1); these are generated every 16 days at 250 m spatial resolution as a Level 3 product and were obtained from NASA's Land Processes Distributed Active Archive Center (LP DAAC) [53]. The meteorological data, which were obtained from the China Meteorological Data Service Center, included the monthly average temperature, monthly total precipitation, and radiation. All spatial input data were transited to the same coordinate system and resampled to the same spatial resolution of 250 m × 250 m. The agricultural production data and urban and rural population data were obtained from the Beijing Statistical Yearbook [48], and the energy and fuel consumption data were obtained from the China Energy Statistical Yearbook [54] and the Beijing Statistical Yearbook [48].

Table 1. Components of the urban carbon metabolism.

Symbol	Component	Composition
C	Cultivated land	Irrigated cultivated land (C1); dry cultivated land (C2)
F	Forest	Forest (F1); shrub land (F2); open woodland (F3); other woodland (F4)
G	Grassland	High-coverage grassland (G1, vegetation cover more than 50%); medium-coverage grassland (G2, vegetation cover between 20 and 50%); low-coverage grassland (G3, vegetation cover between 5 and 20%);
W	Water	Rivers (W1); lakes and reservoirs (W1); intermittently flooded land (W3)
U	Urban land	Built-up areas of the city
R	Rural land	Rural residential areas independent from the urban areas
T	Transportation and industrial land	Large areas of industrial and transportation land outside the urban and rural residential areas
B	Bare land	Unused and non-vegetated land

2.2. Urban Carbon Flows Accounting

- Urban carbon metabolism calculation

Urban carbon metabolism represents the flows of both carbon sequestration and emissions between the biosphere and the atmosphere and the carbon transitions within the components of the urban system. The carbon metabolic density (W) was the carbon metabolic rate per unit area, i.e., the annual carbon metabolism. Two forms were considered for each component: carbon sequestration density (W_S) and carbon emission density (W_E). The carbon transition flow represents the amount of carbon flow from one component of the system to another and is expressed as the difference in carbon metabolic density (ΔW) wherever the land use changed, which can be calculated as follows [55]:

$$\Delta W = W_i - W_j = \left(\frac{V_i}{S_i}\right) - \left(\frac{V_j}{S_j}\right)$$

where i and j represent the final and initial components, respectively; W_i and W_j represent the carbon metabolic density of the final and initial component, respectively; V is the carbon

metabolism rate (kg C yr^{-1}) and can be expressed as either the carbon emission rate (V_E) or the carbon sequestration rate (V_S); S_i and S_j represent the area of component i and j, respectively.

The net direction of the carbon transition flow can be determined by the result: if $\Delta W > 0$, it means carbon sequestration increase or carbon emission decrease, and thus the process is beneficial; if $\Delta W < 0$, it means carbon sequestration decrease or carbon emission increase, and thus the process is harmful. By multiplying the area of land that was transferred between two components by the corresponding ΔW value, the total carbon flow between the two components was calculated. The formula was as follows [55]:

$$f_{ji} = \Delta W \times \Delta S_{ji}$$

where f_{ji} refers to the carbon flow from component j to component i; ΔS_{ij} represents the area of land that is transferred from component j to component i.

- Carbon sequestration evaluation using the Carnegie–Ames–Stanford Approach (CASA) model

Carbon sequestration took place through the photosynthesis of vegetation, and net primary productivity (NPP) was used to characterize the carbon sequestration of urban components. The CASA model calculates regional carbon storage and its spatial distribution on the basis of the photosynthetically active radiation absorbed by vegetation [45]. Carbon sequestration accounting by the CASA model can avoid the limit and inconsistency of traditional station data in regional-scale research. Zhu et al. [46,56] modified the model and localized parameters according to the characteristics of vegetation in China. The carbon sequestration of the urban components in this study was calculated using the modified CASA, which is summarized in the following equation.

$$NPP(x,t) = APAR(x,t) \times \varepsilon(x,t)$$

$$APAR(x,t) = SOL(x,t) \times FPAR(x,t) \times 0.5$$

$$\varepsilon(x,t) = f_1(x,t) \times f_2(x,t) \times W(x,t) \times \varepsilon_{max}$$

where $NPP(x, t)$ refers to the NPP of pixel x in month t; $APAR(x, t)$ (MJ·m^{-2}·month^{-1}) represents the absorbed photosynthetically active radiation of pixel x in month t; $\varepsilon(x, t)$ (g C·MJ^{-1}) represents the light use efficiency of $APAR$ into organic dry matter of pixel x in month t; $FPAR(x, t)$ refers to the fraction of the incoming photosynthetically active radiation absorbed by the vegetation canopy, which depends on the type and coverage of vegetation; $SOL(x, t)$ (MJ·m^{-2}·month^{-1}) represents the total solar radiation; and the constant 0.5 stands for the proportion of solar active radiation used for vegetation to the total solar radiation.

The $FPAR$ is near-linearly correlated with the $NDVI$, and the correlation is determined according to the maximum and minimum $NDVI$ values for a certain vegetation type and the corresponding $FPAR$ values. Some studies have indicated that $FPAR$ is also linearly related to the simple ratio (SR). The mean value of $FPAR$ estimated by the SR-$FPAR$ and $NDVI$-$FPAR$ models was applied in this study to minimize bias [56]. Vegetation has the maximum light use efficiency (ε_{max}) in ideal conditions, but the actual light efficiency (ε) of each pixel is affected by the suitability of temperature and the availability of water. The parameters used in the study came from Zhu et al.'s work [46,56]. Using the CASA model, the NPP of Beijing for the years 2000, 2005, 2010, 2015, and 2020 was calculated with ENVI 5.0 software, and the NPP of each urban component for each year was derived by overlaying the corresponding data on land use type.

- Carbon emission accounting

Carbon emissions for the components of urban land, rural land, transportation and industrial land, and cultivated land were calculated on the basis of the consumption of fuel,

and indirect carbon emissions were not considered in this study. The carbon emission rate calculation for the abovementioned land use types is as follows:

$$v_{EU} = \sum E_{Ui} K_i + k_0 P_u$$

$$v_{ER} = \sum E_{Ri} K_i + k_0 P_r$$

$$v_{ET} = \sum E_{Ti} K_i$$

$$v_{EC} = v_{ECF} + v_{ECM} + v_{ECI} + v_{ECL} = k_1 F + k_2 M + k_3 S_i + k_4 P_i + k_5 C_a$$

v_{EU} is the carbon emission rate of urban land; E_{Ui} is the energy consumption of urban households, the construction industry, and other service industries; K_i is the carbon emission coefficient of the ith energy; k_0 is the carbon emission coefficient of human breathing; P_u is the urban population.

v_{ER} is the carbon emission rate of rural land; E_{Ri} is the energy consumption of rural households; P_r is the rural population.

v_{ET} is the carbon emission rate of transportation and industrial land; E_{Ti} is the energy consumption of the mining and manufacturing industries and transportation, storage, postal, and telecommunications services.

v_{EC} is the carbon emission rate of cultivated land, which includes the carbon emission rate for fertilizers (v_{ECF}), farming machinery (v_{ECM}), irrigation (v_{ECI}), and livestock (v_{ECL}), respectively. F is the amount of fertilizer; M is the mechanical power of the agricultural equipment; S_i is the irrigated area; P_i and C_a are the quantities of pigs and cattle. k_1, k_2, k_3, k_4, and k_5 are the carbon emission coefficients of the corresponding items. All the values and references of the coefficients are summarized in the Supplementary Materials (Tables S1–S3).

2.3. Spatial Pattern of Carbon Metabolism

To describe the detailed spatial patterns of carbon metabolism and the associated flows, we obtained the land transformation matrix in four time intervals (2000–2005, 2005–2010, 2010–2015, and 2015–2020) to allocate the corresponding carbon metabolism changes of each component of the city using ArcGIS 10.3.

3. Results

3.1. Land Use Change of Beijing during 2000~2020

In the past two decades, Beijing has witnessed a rapid urbanization process, primarily characterized by the significant expansion of construction land and the shrinkage of cultivated land (Figure 2, Table S4). Construction land, containing urban land, rural land, transportation land, and industrial land, reached 3471.57 km^2 in 2020, an increase of 55% from 2000. Urban land increased from 1035.01 km^2 in 2000 to 1494.37 km^2 in 2020, with an annual expansion of 22.97 km^2 yr^{-1}. Meanwhile, cultivated land dramatically decreased from 4914.20 km^2 in 2000 to 3765.47 km^2 in 2020, with an annual shrinkage of 57.44 km^2 yr^{-1}. The annual changes in forest, grassland, and water area ranged from 3.5 km^2 yr^{-1} to 5.5 km^2 yr^{-1}, which were smaller than the changes in cultivated land and construction land.

The urban expansion in Beijing was inextricably associated with the cultivated land loss since newly built-up areas predominantly occupied cultivated land in former rural areas. The land transformation matrix for the past two decades also showed that the conversion of cultivated land to construction land has continuously been the predominant direction of land use transformation. Over 90% of the lost cultivated land was converted to construction land in 2000–2005 and 2005–2010, and the proportion declined to 75.5% and 53.0% in 2000–2005 and 2005–2010, respectively. Cultivated land was also converted to

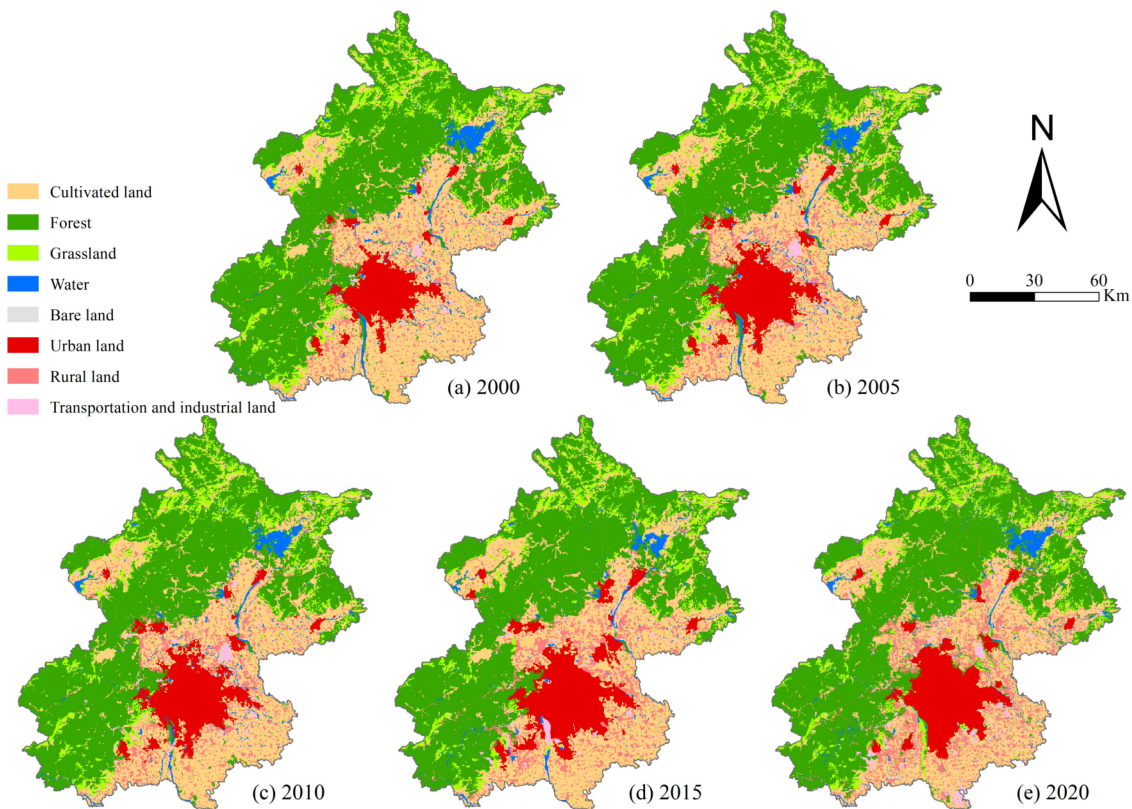forest in the past decade, and the area of cultivated land converted to forest was 188.46 km^2 in 2015–2020.

Figure 2. Land use map in Beijing in 2000 (**a**), 2005 (**b**), 2010 (**c**), 2015 (**d**) and 2020 (**e**).

3.2. Spatiotemporal Changes of Carbon Emissions and Sequestration

Carbon emissions of the four components, namely urban, rural, transportation and industrial, and cultivated land, experienced a similar trend of first increasing and then decreasing (Figure 3). The total carbon emission rate of Beijing increased from 2211.31 $\times$ 10^7 kg C yr^{-1} in 2000 to 2532.85 $\times$ 10^7 kg C yr^{-1} in 2010 and declined to 1764.31 $\times$ 10^7 kg C yr^{-1} in 2020. In 2000, transportation and industrial land was the top contributor to the city's carbon emissions, contributing 62.8% of the total emissions with only 1.28% of the city's area, followed by urban land, which accounted for 24.1% of the total emissions. The carbon emission intensity of urban land was 5.15 $\times$ 10^6 kg C km^{-2} yr^{-1}, which was only 7.8% of the value of transportation and industrial land. The carbon emissions of urban land increased to 1116.49 $\times$ 10^7 kg C yr^{-1} in 2015 and subsequently decreased to 965.31 kg C yr^{-1} in 2020. The proportion of carbon emissions from urban land to total emissions increased to 54.7%, surpassing that from transportation and industrial land (636.45 $\times$ 10^7 kg C yr^{-1}, 36.1%) and becoming the top contributor of carbon emissions in 2020. In addition, the carbon emissions from rural land increased from 150.41 $\times$ 10^7 kg C yr^{-1} in 2000 to 196.8 $\times$ 10^7 kg C yr^{-1} in 2010 and decreased to 118.43 $\times$ 10^7 kg C yr^{-1} in 2020. The proportion of carbon emissions from rural land to the city's total ranged from 6% to 8% in 2000~2020, and the carbon emission intensity decreased from 1.51 $\times$ 10^6 kg C km^{-2} yr^{-1} in 2000 to 0.72 $\times$ 10^6 kg C km^{-2} yr^{-1} in 2020. Meanwhile, although cultivated land was the largest of the four carbon emission components, accounting for more than 22% of the city's area, its carbon emission rate was the lowest and continuously declined from 138.93 $\times$ 10^7 kg C yr^{-1} to 44.12 $\times$ 10^7 kg C yr^{-1} from 2000 to 2020.
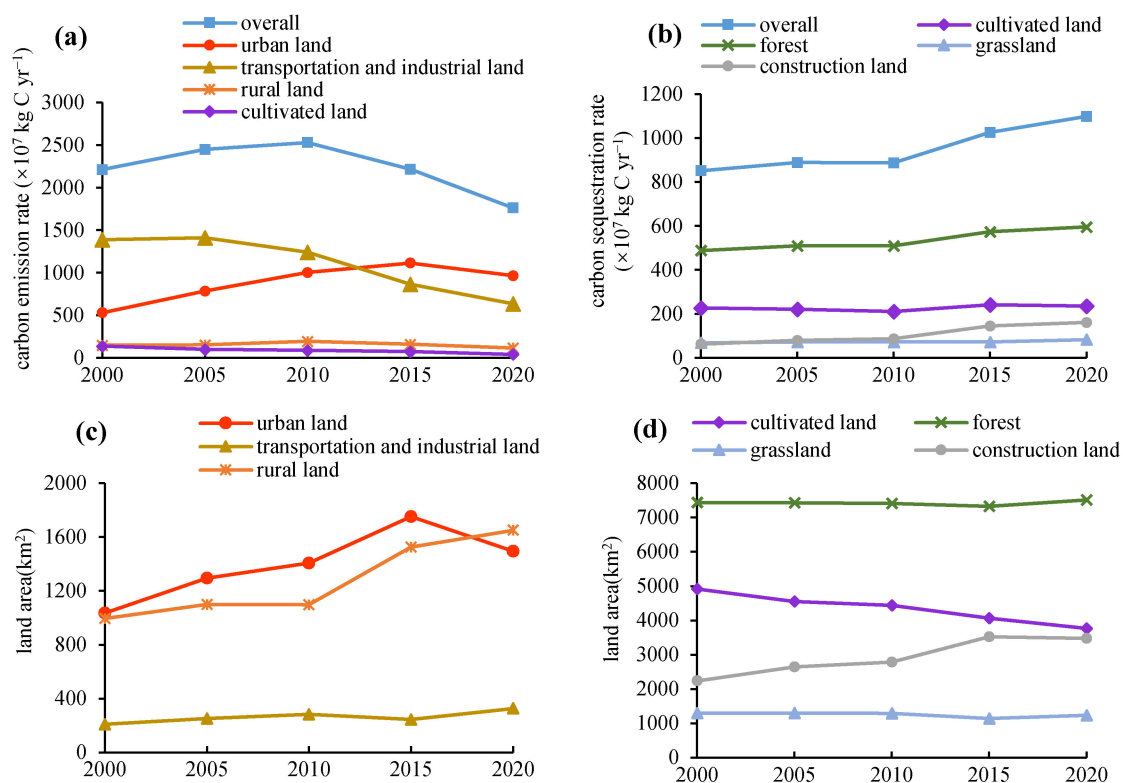
Figure 3. Changes in (**a**) carbon emission rates and (**b**) carbon sequestration rates and the land area of the main contributors to (**c**) carbon emission and (**d**) carbon sequestration in Beijing from 2000 to 2020.

Compared with the carbon emission rate, the carbon sequestration rate in Beijing was relatively lower and could not balance the carbon metabolism of the city. The CASA model estimation results showed that the total carbon sequestration rate of Beijing increased from 851.85×10^7 kg C yr^{-1} in 2000 to 1098.70×10^7 kg C yr^{-1} in 2020, with an average annual increase of 12.34×10^7 kg C yr^{-1}. Forest land contributed the lion's share of the city's carbon sequestration from 2000 to 2020 due to the combination of the largest area and the highest carbon sequestration density, accounting for about 55% of the city's total carbon sequestration during the study period. Among its four sub-components (forest land, shrub land, open woodland, and other woodland), forest land was the top contributor, and its carbon sequestration reached 398.57×10^7 kg C yr^{-1} in 2020. Cultivated land was the second-largest contributor to the city's carbon sequestration and accounted for about 21.3% of the total carbon sequestration rate. Grasslands had a higher carbon sequestration density than cultivated land, but their sequestration rate accounted for only 7.6% of the total since their area was much lower than that of cultivated land.

The carbon metabolism of Beijing showed a spatial gradient distribution from the central plain area of the city to the inner suburban area and then to the outer suburbs of the mountains, presenting a downward trend from the southeast plains to the northwest mountains overall (Figure 4). Carbon emissions gradually decreased along this gradient, while the carbon sequestration rate increased from the southeast to the northwest. The central urban area in the southeast plain was the area with the highest carbon emission rate and the lowest carbon sequestration rate in the city, and the distribution was highly concentrated. By contrast, the northwest mountainous area was the area with the highest carbon sequestration rate and the lowest carbon emission rate, while the distribution was more disaggregated. The inner suburban area in the periphery of the southeast plain had middling carbon emission and sequestration rates compared with the other two regions, and it was a transition zone of spatial disaggregation and aggregation distribution of carbon metabolism.
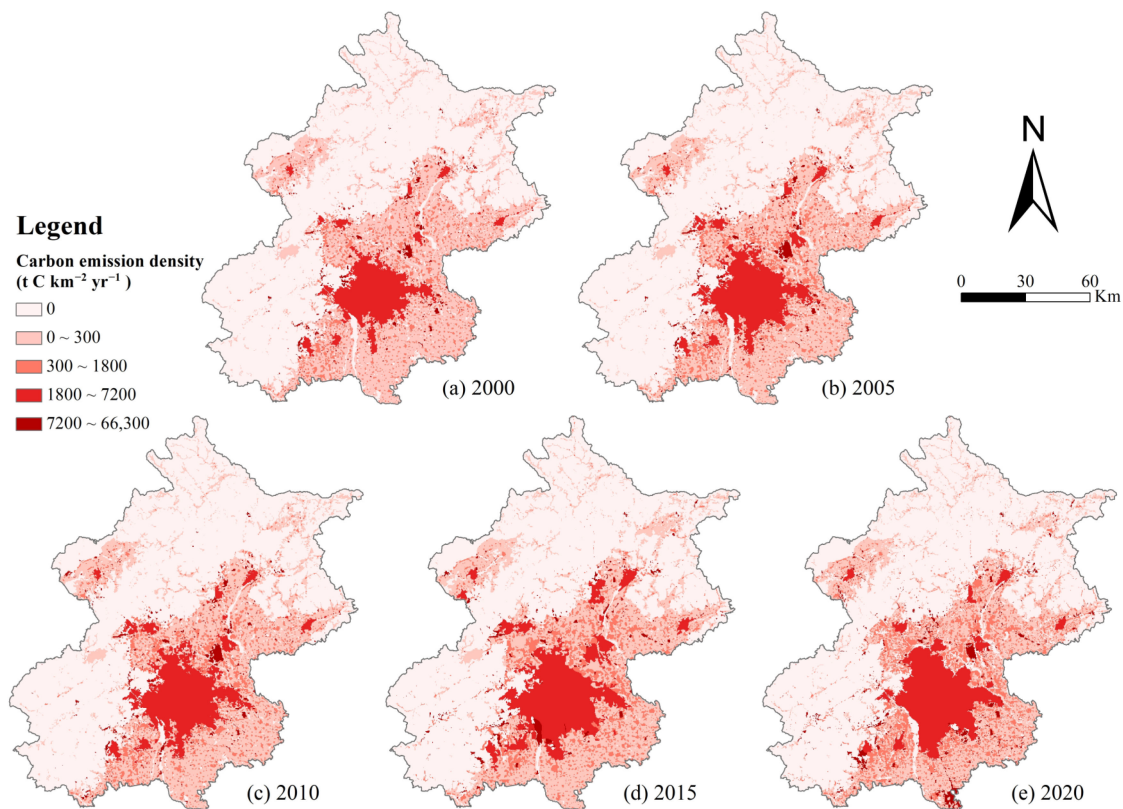
Figure 4. Spatial patterns of carbon emissions of Beijing in 2000 (**a**), 2005 (**b**), 2010 (**c**), 2015 (**d**) and 2020 (**e**).

Until 2015, the urban area in the southeast plain with high carbon emissions (1.8×10^6–66.3×10^6 kg C km^{-2} yr^{-1}) showed notable infilling and expansion, and the density increased. The patches with moderate carbon emissions (0.3×10^6–1.8×10^6 kg C km^{-2} yr^{-1}), which were embedded in the low-carbon patches (0–0.3×10^6 kg C km^{-2} yr^{-1}) in the periphery of the southeast plain, expanded and spatially aggregated. The dominant low-carbon patches in the periphery of the southeast plain were simultaneously fragmented overall but aggregated in several local areas. After 2015, the patches with high carbon emissions in the central urban area shrank slightly, whereas some patches with high emissions emerged in local areas, such as in the south of Daxing District, where Beijing Daxing International Airport was constructed and put into operation in 2019.

During the first half of the study period, the spatial distribution of carbon sequestration in the northwest mountains was relatively stable and did not show the highly aggregated distribution that the high-carbon emission zone did (Figure 5), and only a few small-scale clusters of patches with the highest carbon sequestration (0.75×10^6–1.1×10^6 kg C km^{-2} yr^{-1}) existed and intensified in some local areas. The periphery of the southeast plain was dominated by patches with moderate carbon sequestration (0.4×10^6–0.6×10^6 kg C km^{-2} yr^{-1}), which were simultaneously fragmented overall. The patches with low carbon sequestration (0–0.4×10^6 kg C km^{-2} yr^{-1}) embedded in the patches with moderate carbon expanded and spatially aggregated. The dominant patches with low carbon sequestration in the urban area in the southeast plain also increased and expanded. After 2010, the dominant patch in the northwest mountains gradually changed from the second highest (0.6×10^6–0.75×10^6 kg C km^{-2} yr^{-1}) to the highest (0.75×10^6–1.1×10^6 kg C km^{-2} yr^{-1}) carbon sequestration patches, and the spatial distribution was still disaggregated. In the periphery of the southeast plain, the patches with low carbon sequestration embedded in the moderate-carbon patches decreased and gradually changed to patches with moderate/low carbon sequestration (0.4×10^6–0.5×10^6 kg C km^{-2} yr^{-1}), causing the dominant patches with moderate carbon sequestration to increase and their degree of fragmentation

to decrease. The dominant patches with low carbon sequestration in the urban area in the southeast plain decreased and gradually changed to patches with moderate/low carbon sequestration, resulting in the decrease in size and the increase in fragmentation.
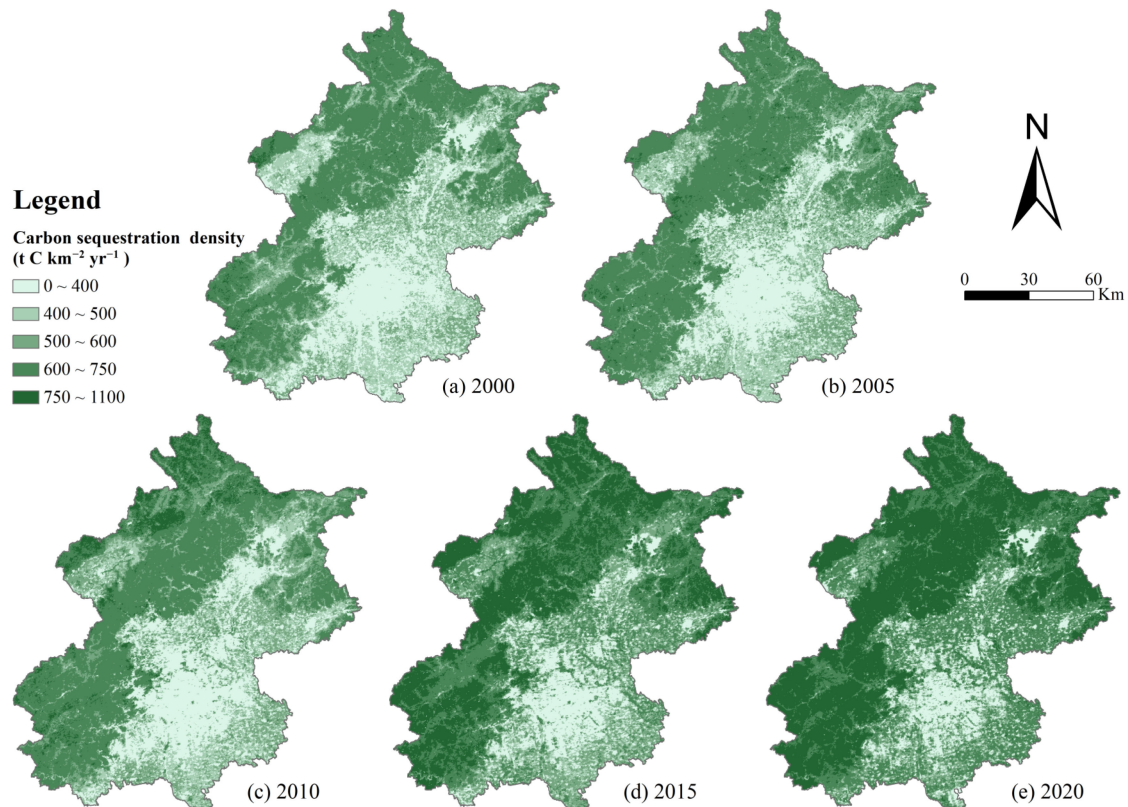

Figure 5. Spatial patterns of carbon sequestration of Beijing in 2000 (**a**), 2005 (**b**), 2010 (**c**), 2015 (**d**) and 2020 (**e**).

3.3. Carbon Transition between Urban Components

Table 2 summarizes the main carbon flow processes between urban components in Beijing in 2000~2020. The overall carbon transition pattern in Beijing was the increase in emissions before 2010 and the decrease in emissions after 2010. The net carbon transition rate showed a carbon emission increase of 295.06×10^7 kg C yr^{-1} from 2000 to 2005 and an increment decline to 131.40×10^7 kg C yr^{-1} from 2005 to 2010. Carbon emissions decreased 60.97×10^7 kg C yr^{-1} and 166.36×10^7 kg C yr^{-1} from 2010 to 2015 and from 2015 to 2020, respectively. From 2000 to 2005, the total harmful carbon transition reached 343.37×10^7 kg C yr^{-1}, nearly 7.12 times the beneficial effect caused by carbon transitions during the same period, bringing the largest gap between the harmful effect and the beneficial effect during the four periods. The carbon transition between cultivated land and transportation and industrial land (168.17×10^7 kg C yr^{-1}) was the top contributor to harmful carbon transitions, followed by the carbon transition between cultivated land and urban land, accounting for 48.98% of the total harmful carbon transition rate in this phase. From 2005 to 2010, the harmful carbon transition rate decreased, while the beneficial carbon transition rate increased. The carbon transition rate between cultivated land and transportation and industrial land decreased to 70.57×10^7 kg C yr^{-1}, and its proportion of the total harmful carbon transition rate reduced to 37.43%.

Table 2. Main carbon transition processes between urban components of Beijing from 2000 to 2020.

Process	2000~2005		2005~2010		2010~2015		2015~2020	
$\times 10^7$ kg C yr^{-1}	Transition Value	Direction	Transition Value	Direction	Transition Value	Direction	Transition Value	Direction
Harmful processes	343.37	−	188.52	−	327.67	−	132.68	−
Beneficial processes	48.31	+	57.11	+	388.64	+	299.04	+
Net transition processes	295.06	−	131.40	−	60.97	+	166.36	+
P1 (C, F)	0.41	C → F+	0.01	C → F+	3.27	C → F+	7.39	C → F+
P2 (C, G)	0.07	C → G+	-	-	1.36	C → G+	3.46	C → G+
P3 (C, W)	0.07	W → C−	0.01	C → W+	1.12	C → W+	0.32	C → W+
P4 (C, U)	87.24	C → U−	30.60	C → U−	78.93	C → U−	2.28	C → U−
P5 (C, R)	9.83	C → R−	2.49	C → R−	2.71	R → C+	10.23	R → C+
P6 (C, T)	168.17	C → T−	70.57	C → T−	46.66	C → T−	103.59	C → T−
P7 (F, G)	0.03	F → G+	-	-	2.83	F → G+	0.16	F → G+
P8 (F, U)	3.83	F → U−	2.70	F → U−	14.87	F → U−	9.71	U → F+
P9 (F, R)	0.86	F → R−	0.35	F → R−	2.51	F → R−	2.88	R → F+
P10 (F, T)	16.85	F → T−	18.21	F → T−	126.80	F → T−	40.13	T → F+
P11 (G, U)	0.46	G → U−	1.26	G → U−	2.95	U → G+	16.57	U → G+
P12 (G, T)	5.28	G → T−	17.93	G → T−	7.55	G → T−	85.65	T → G+
P13 (W, U)	2.53	W → U−	3.88	W → U−	3.32	W → U−	3.77	U → W+
P14 (W, T)	14.31	W → T−	20.12	W → T−	24.80	W → T−	8.47	T → W+
P15 (U, R)	30.03	R → U−	20.39	R → U−	21.22	R → U−	89.05	U → R+
P16 (U, T)	47.59	T → U+	44.15	T → U+	204.12	T → U+	26.82	U → T−
P17 (R, T)	3.62	R → T−	12.95	T → R+	169.42	T → R+	15.78	T → R+
P18 (B, T)	-	-	-	-	0.44	B → T−	2.90	T → B+

Note: Carbon transition processes lower than 1.00×10^7 kg C yr^{-1} through the four periods are not listed in the table. "+" represent beneficial direction with carbon sequestration increase or carbon emission decrease; "−" represent harmful direction with carbon sequestration decrease or carbon emission increase.

After 2010, the beneficial carbon transition rate exceeded the harmful carbon transition rate, and the net processes indicated that carbon emissions decreased beneficially. From 2010 to 2015, the total beneficial carbon transition was the highest during the four periods, reaching 388.64×10^7 kg C yr^{-1}. The carbon transitions between transportation and industrial land and urban land (204.12×10^7 kg C yr^{-1}) and between transportation and industrial land and rural land (169.42×10^7 kg C yr^{-1}) were the main contributors to the beneficial carbon transitions because of the large carbon metabolism density differences, i.e., 36.87×10^6 kg C km^{-2} yr^{-1} and 39.17×10^6 kg C km^{-2} yr^{-1}, respectively. The carbon transition between forest land and transportation and industrial land (126.80×10^7 kg C yr^{-1}) was the top contributor to harmful carbon transitions, followed by the carbon transition between cultivated land and urban land (78.93×10^7 kg C yr^{-1}). From 2015 to 2020, both the harmful and beneficial carbon transition rates were lower than those in the previous five years, while the net carbon transition increased. The main beneficial carbon transitions occurred between urban land and rural land, between transportation and industrial land and grassland, and between transportation and industrial land and forest land. The carbon transition between cultivated land and transportation and industrial land (103.59×10^7 kg C yr^{-1}) was the top contributor to harmful processes, accounting for 78.07% of the total harmful carbon transition rate in the past five years. During the whole study period, the primary carbon transitions in Beijing usually occurred between components greatly affected by human activities, such as transportation and industrial land, due to the high carbon metabolism density. Meanwhile, the carbon transition between cultivated and urban land was also a major contributor because of the remarkable urban expansion during the rapid urbanization process.

3.4. Spatial Pattern of Urban Carbon Metabolism and Its Relationship to Land Use Change

The spatial pattern of the beneficial and harmful carbon metabolism effects of land use transitions during the study period is shown in Figure 6. During the first half of the study period, the harmful carbon transitions mainly occurred in and around the centers of the southeast plain and some northwest mountainous districts. In the above regions, the harmful carbon transition processes (e.g., C → T, C → U, C → R, and U → T) led to the expansion of patches with high carbon emissions and low carbon sequestration. Moreover, the urban land that remained unconverted also showed harmful carbon effects since the carbon emissions of the urban sector rapidly increased from 2000 to 2010. From 2010 to 2015, the unconverted urban land in the center of the southeast plain showed beneficial carbon effects, mainly due to the decrease in the carbon emission density since the increment in urban carbon emissions was lower than the increase in the urban land area. The transitions with harmful carbon effects, which mainly included C → U, F → U, and R → U, continuously led to the local expansion of patches with high carbon emissions in all directions around the central urban area of the southeast plain. Meanwhile, some transitions with beneficial carbon effects in the outer suburbs brought carbon sequestration recovery (e.g., C → F and G → F) and carbon emission reduction (e.g., U → R, T → U, and T → R). From 2015 to 2020, the main harmful carbon transition processes (e.g., C → T, C → U, and R → U) in the southeast plains led to the constant expansion of patches with high carbon emissions, especially in the south Daxing District, where Beijing Daxing International Airport is located. Around the center of the southeast plain, the beneficial carbon transition processes (e.g., U → R) led to the shrinkage of patches with high carbon emissions and low carbon sequestration. In the periphery of the southeast plain, where rural land is embedded in cultivated land, the land use type that remained unchanged also showed beneficial carbon effects, mainly because the carbon emissions of both rural and agricultural sectors decreased from 2015 to 2020, resulting in the recovery of patches with moderate sequestration and the decrease in their spatial fragmentation. In the northwest mountainous region dominated by forest and grassland, land use types that remained unchanged generally showed beneficial carbon effects in most periods from 2000 to 2020 since the carbon sequestration density of most patches increased while some patches decreased locally.

As summarized in Table 3, the net gross carbon transition rate of land use change in Beijing turned from emissions increasing by 237.03×10^7 kg C yr^{-1} in 2000~2005 to emissions decreasing by 420.99×10^7 kg C yr^{-1} in 2015~2020. The land use conversion in Beijing overall had a harmful carbon effect before 2010 and a beneficial carbon effect after 2010, while the land use type that remained unchanged overall showed a beneficial carbon effect constantly from 2000 to 2020. The conversion of cultivated land to construction land was the dominant harmful carbon transition process during the study period, especially the conversion from cultivated land to transportation and industrial land (C → T) and urban land (C → U). The largest gap between the harmful and beneficial carbon effects of land use conversion happened from 2000 to 2005, corresponding to a substantial amount of the land use conversion above. From 2015 to 2020, the decrease in the construction of new industrial facilities and the reduction in urban expansion partly offset the rapid increase in the carbon emission density of construction land, which led to a slight increase in harmful carbon effects. In addition, the conversions from transportation and industrial land to urban land (T → U) and rural land (T → R) were important beneficial carbon transition processes, bringing marked reductions in carbon emissions since the carbon emission density of transportation and industrial land was much higher than that of the other two kinds of constriction land. For the land use type that remained unchanged, the overall net carbon effect showed that carbon emission reduction decreased by 58.03×10^7 kg C yr^{-1} from 2000 to 2005, and the decrement increased to 356.20×10^7 kg C yr^{-1} from 2010 to 2015 and then subsequently fell to 254.63×10^7 kg C yr^{-1} from 2015 to 2020. Both forest land and grassland that remained unchanged embodied more beneficial carbon effects after 2010 than before 2010 since the carbon sequestration density significantly increased after 2010.

Construction land (U, R, T) that remained unchanged showed beneficial carbon effects after 2010 because the carbon emission density decreased, and the carbon sequestration increased simultaneously.

Table 3. Main carbon flows of land use transition processes in Beijing from 2000 to 2020.

Process	2000~2005		2005~2010		2010~2015		2015~2020	
$\times 10^7$ kg C yr^{-1}	Transition Value	Direction/ Proportion	Transition Value	Direction/ Proportion	Transition Value	Direction/ Proportion	Transition Value	Direction/ Proportion
Land use transition processes	295.06	−	131.40	−	60.97	+	166.36	+
Harmful processes								
C → U−	−87.24	24.25%	−30.60	16.04%	−105.93	14.12%	−49.11	11.93%
C → R−	−9.83	2.73%	−2.50	1.31%	−14.36	1.91%	−3.50	0.85%
C → T−	−169.00	46.97%	−70.57	37.00%	−193.60	25.80%	−163.99	39.85%
F → U−	−3.83	1.07%	−2.70	1.42%	−15.00	2.00%	−1.58	0.38%
F → T−	−16.85	4.68%	−18.21	9.55%	−164.02	21.86%	−13.99	3.40%
G → T−	−5.28	1.47%	−17.93	9.40%	−59.06	7.87%	−32.57	7.91%
W → U−	−2.66	0.74%	−3.91	2.05%	−6.55	0.87%	−2.50	0.61%
W → T−	−14.72	4.09%	−20.47	10.73%	−45.08	6.01%	−6.25	1.52%
U → T−	-	-	−0.48	-	−35.08	-	−54.17	-
R → U−	−30.05	8.35%	−20.39	10.69%	−46.84	6.24%	−29.73	7.23%
R → T−	−18.58	5.16%	−1.34	0.70%	−53.10	7.08%	−49.15	11.94%
Beneficial processes								
C → F+	0.41	0.63%	0.01	0.01%	5.91	0.73%	6.76	1.17%
C → G+	0.07	0.11%	-	-	1.98	0.24%	2.17	0.38%
C → W+	0.02	0.03%	0.01	0.02%	1.48	0.18%	0.30	0.05%
G → F+	0.02	0.04%	-	-	2.73	0.34%	2.57	0.44%
U → C+	-	-	-	-	27.01	3.33%	46.83	8.10%
U → F+	-	-	-	-	0.14	0.02%	11.29	1.95%
U → G+	-	-	-	-	4.86	0.60%	18.22	3.15%
U → W+	0.13	0.20%	0.04	0.06%	3.23	0.40%	6.27	1.08%
U → R+	0.02	0.04%	-	-	25.62	3.16%	118.78	20.55%
R → C+	-	-	0.01	0.01%	17.06	2.10%	13.74	2.38%
T → C+	0.83	1.28%	-	-	146.94	18.11%	60.40	10.45%
T → F+	0.00	0.00%	-	-	37.22	4.59%	54.12	9.37%
T → G+	-	-	-	-	51.51	6.35%	118.22	20.46%
T → W+	0.41	0.64%	0.35	0.59%	20.28	2.50%	14.72	2.55%
T → U+	47.59	73.55%	44.62	75.21%	239.20	29.48%	27.35	4.73%
T → R+	14.96	23.12%	14.29	24.08%	222.53	27.43%	64.94	11.24%
Land use type unchanged	58.03	+	16.59	+	356.20	+	254.63	+
C → C	12.69	−	20.44	−	87.49	+	53.72	+
F → F	20.24	+	2.78	−	60.26	+	51.20	+
G → G	2.00	+	0.07	−	8.23	+	10.32	+
W → W	0.71	+	1.22	−	2.68	+	4.31	+
B → B	0.00	−	0.00	−	0.00	+	0.00	+
U → U	96.55	−	137.02	−	112.07	+	3.49	−
R → R	7.67	+	37.42	−	57.71	+	36.00	+
T → T	136.65	+	215.54	+	27.75	+	102.57	+
Total	237.03	−	114.82	−	417.16	+	420.99	+

Note: "+" represent beneficial direction with carbon sequestration increase or carbon emission decrease; "−" represent harmful direction with carbon sequestration decrease or carbon emission increase.
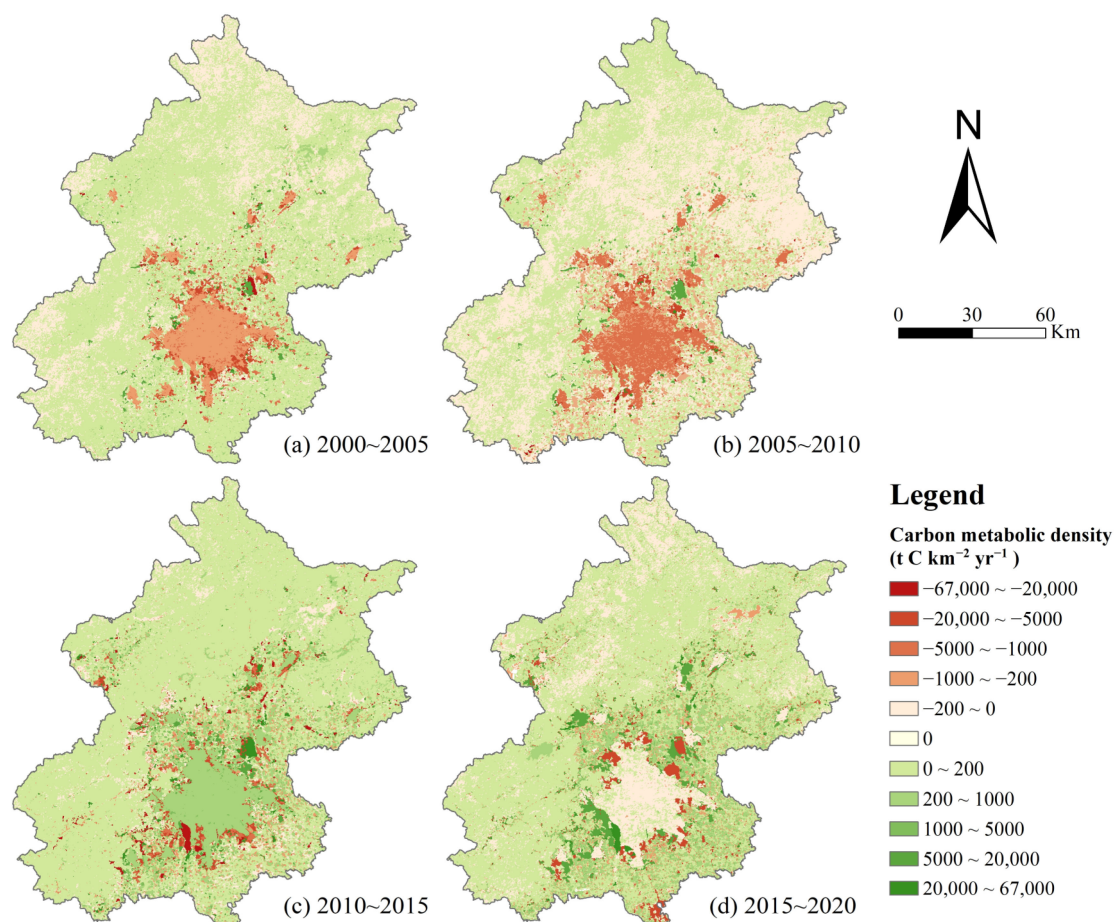
Figure 6. Spatial patterns of beneficial (+) and harmful (−) carbon transitions in Beijing from 2000 to 2005 (**a**), from 2005 to 2010 (**b**), from 2010 to 2015 (**c**) and from 2015 to 2020 (**d**).

4. Discussion

4.1. Urban Carbon Metabolism with Land Use Change and Urban Development Policies

From 2000 to 2020, both the carbon emission rate and the net carbon emission rate increased in the first decade and decreased in the next, while the carbon sequestration rate kept rising. The net carbon emission rate of Beijing averaged 1284.52×10^7 kg C yr^{-1}, indicating that the entire system of the city has been functioning as a net carbon source rather than a carbon sink. This rate decreased by 34.69×10^7 kg C yr^{-1}, caused by land use change during the study period, which amounted to 1.5% of the overall carbon emission rate. Although the amount was very limited compared with total carbon emissions, the overall change in carbon flux caused by land use change was beneficial during the study period. The above positive influence was closely related to land use policy development. For instance, a national carbon-control target was set by the central government of China in 2009 and has been gradually incorporated into the performance appraisal system of local governments. This policy had many positive influences on carbon emission reduction in many areas in China.

The highest harmful carbon flows were mainly from the conversion of natural components to artificial components, which led to a sharp decline in carbon sequestration and a simultaneous increase in carbon emissions. The transformation from cultivated land to industrial and transportation land and urban land led to typical harmful carbon flows during the study period. Hence, promoting the intensive use of construction land and carefully considering occupying cultivated land with construction land is necessary for future urban spatial planning and land use management. As for the beneficial carbon flows, the conversion of transportation and industrial land, which had the highest carbon

emission density, to urban land (T → U) and rural land (T → R) led to carbon emission reduction. Another noteworthy positive carbon flow was the land use transfer out of and into forest land or grassland. In 2012, Beijing launched the "one-million-mu afforestation and greening project in plain areas"; a total of 1.05 million mu were afforested and more than 54 million trees were planted by 2015. The forest coverage rate in the whole city of Beijing increased from 37.6% to 41%, and the rate in the plain area increased from 14.85% to 25%. In 2018, Beijing implemented another round of the "one-million-mu afforestation project in plain areas" and completed more than 0.69 mu of new afforestation by 2020. In particular, priority was given to the afforestation of vacated urban land, abandoned opencast mines, tidal flats, and sand wastelands in the two rounds of the project construction. The impact of the above project was well-reflected in our study, which showed that the positive carbon flows resulting from the conversion from other land to forest land and grassland greatly increased after 2010 compared with that before 2010.

In addition to the carbon flows caused by the land use type transformation, this study also assessed the carbon metabolism of the unconverted land use type. The unconverted natural components showed a beneficial carbon process overall, indicating that the carbon sequestration density of untransformed forest land and grassland increased during the study period. The carbon metabolism of untransformed cultivated land was harmful before 2010 but beneficial after 2010. It was associated with the conversion within cultivated land. The Beijing municipal government implemented a series of water-saving measures in response to the city's water shortage. In particular, the rural agricultural structure adjustments, which included reducing the planting area of water-intensive crops, such as rice and winter wheat, was given high priorities. The area of conversion from paddy fields to dry land was larger after 2010 than before, bringing a marked decline in carbon emissions. The overall carbon metabolism of unconverted construction land was beneficial, as the increasing carbon sequestration intensity could offset the carbon emission intensity growth of individual land use types. In the master planning and the 12th and 13th Five-Year Plans of Beijing, the general idea of green, low-carbon, and circular development was established, and a series of measures was continuously introduced to achieve the high-standard goals and tasks. The proportion of coal consumption in the city's energy consumption decreased from 25.2% in 2012 to less than 1.5% in 2020. The carbon emission intensity of transportation and industrial land steadily declined during the study period with the adjustment of the energy consumption structure.

The study also analyzed the spatial characteristics of urban carbon metabolism with land use change and found that the zones of high negative carbon transitions gradually shifted outward from places close to the city center. This trend of the main negative carbon effects always being transferred to less developed regions has also been found by other studies on Beijing and Hangzhou. With the development of urban progress, the city was filled, and some industries had to be transferred outward, leading to an industrial carbon transfer and an increase in carbon emissions in the region where these industries relocated. In the mountainous region far from the city center, the carbon metabolism caused by land use change overall was beneficial throughout the study period. Therefore, policies must consider regional differences; for example, regulating carbon emissions should be prioritized in urban areas with high concentrations of population and industries, while increasing carbon storage should be emphasized in suburban areas and mountainous areas far from the city center. Moreover, some market eco-compensation approaches, such as a carbon trading market, may help curb carbon emissions and enhance carbon sinks more efficiently in the corresponding key areas.

4.2. Comparison with Other Studies

As the capital of China, Beijing is one of the largest metropolises by both area and population in China and has been a hot region of previous studies on urban carbon metabolism. Zhang et al. evaluated the carbon emission and sequestration rates, analyzed their spatial patterns, and quantified carbon flows caused by land use changes

from 1990 to 2008. The growth rate of carbon emissions from 2005 to 2008 was lower than the growth from 2000 to 2005, and this was consistent with the change trend of the carbon emissions from 2000 to 2010 in our study. In Zhang's [40] study, the overall carbon sequestration was 39.41×10^7 kg C yr^{-1} in 2008, which was quite a bit lower than that in our study. This was mainly caused by the differences in the concept scope and the assessment method. Zhang estimated the carbon sequestration rate of only four components (forest, grassland, water, and cultivated land) using empirical carbon sequestration coefficients, while our study evaluated the net primary production of all kinds of urban components in the whole city using the CASA model. The carbon sequestration coefficients used in Zhang's [40] study were far lower than the carbon sequestration density obtained by the CASA model in this study. However, the NPP estimated in this study was, in general, consistent with that of other published studies [57]. The Institute of Geographic Sciences and Natural Resources Research of the Chinese Academy of Sciences published a set of NPP data with a spatial resolution of 1 km $\times$ 1 km for China from 2000 to 2010 based on the GLO_PEM model [58]. In this set of data, the NPP of urban construction land and bare land was excluded. We extracted the data of Beijing, and the average NPP of the city in 2000 and 2010 was 0.48×10^6 kg C km^{-2} yr^{-1} and 0.56×10^6 kg C km^{-2} yr^{-1}, respectively. The quantity and the increasing trend were consistent with the results of this study. Compared with the MOD17A3HGFv061 [59] product at 500 m resolution from MODIS, the NPP results in this study were higher, while the increasing trend and the spatial characteristics were consistent. The disparity between MOD17A3HGFv061 and this study in mountainous areas was more distinct than that in the plain areas, reflecting that the model accuracy is impacted by complexity in vegetation structure, temperature, humidity, and precipitation in mountainous areas with a large degree of relief [47].

Compared with urban metabolism in other cities, the results exhibited a high dispersion associated with the differences in the energy consumption structure and land use patterns. However, some similar characteristics were still found. Our study discovered that conversions from transportation and industrial land to urban land (T $\rightarrow$ U) and rural land (T $\rightarrow$ R) near the urban center in the southeast plain area and the conversion from cultivated land to forest land in the northwestern mountains were important beneficial carbon transition processes in Beijing. Similar studies in Hangzhou [33,41] and the Yangtze River Delta [60] showed a similar trend, in which the most beneficial carbon transitions were in the urban central area, where existing industries were gradually removed, and the western mountainous areas, which benefited from the Grain for Green Project. Although topographic factors could have affected the spatial pattern of urban carbon metabolism, the shift of zones with high negative carbon transitions from well-developed regions to less developed regions seemed to be a common feature.

4.3. Limitations of the Study and Perspective for Future Research

In this study, NPP was used to represent the carbon sequestration rate of the urban components, and the respiratory consumption of heterotrophs was not eliminated. Thus, the carbon sequestration estimation results may be higher than those of other studies. The NPP value of non-vegetated areas, such as water bodies (lakes and rivers), should be zero, while the NPP value estimated in the paper is relatively high. It was partly determined by the spatial resolution of the remote sensing data. For NDVI and LUCC data with a spatial resolution of 250 m $\times$ 250 m, some narrow streams and small ponds cannot be well identified. Another reason is the problem of mixing pixels. A mixed pixel of water and vegetation may be classified as water if the proportion of water is relatively large but also contains vegetation components, and it may be shown as a certain NDVI value (not zero) in the remote sensing data. Similar situations also include the mixed pixels of construction land and natural components. For instance, urban green space is a typical mixed pixel of impervious surface and trees or shrubs and may result in a higher NDVI value than that of pure construction land. Another limitation lies in the rough estimation of the light energy utilization, which impacts the accuracy of the NPP results, especially

in the mountainous region, where the vegetation structure, temperature, humidity, and precipitation show great differences [47]. Moreover, the respiration rate of ecosystem heterotrophs was not eliminated, so the results were larger than those of other studies on urban carbon metabolism. However, estimating NPP with the CASA model could effectively estimate regional carbon sequestration status in different periods, reflecting the differences in the same urban component in the same place at different times and in different places at the same time especially well by relating environmental variables to vegetation. On the premise of giving full consideration to the above methodological limitations and advantages, the results of this work should be interpreted with analytical caution.

This study revealed the spatial pattern of urban carbon metabolism with land use change in Beijing over the past two decades. The urban system was divided into eight rough components, and the reallocation of carbon emission subsectors into the corresponding individual land use types was relatively coarse due to the lack of a clear relationship between them. Thus, further study could build a land use data set with a finer spatial and temporal resolution to accommodate the more detailed socioeconomic data. The carbon emission difference of the same land use type in different regions was not considered due to the data limitations. A refined carbon emission allocation of the same urban component to different areas is ideal for accounting for transboundary carbon transitions more accurately. As for the methodology, the improvement of the accuracy of the CASA model will contribute to the understanding of the regional carbon status more precisely. In addition, the influential factors of urban metabolism and the driving mechanism are issues worthy of further study. The simulation of urban carbon metabolism associated with projected land use changes in different scenarios is also well worth studying since the modeling results could provide decision-makers with more detailed information to formulate urban low-carbon development measures.

5. Conclusions

This study presents an attempt to combine the CASA modeling and empirical co-efficients in an urban carbon metabolism analysis. According to the evaluation of the temporal changes in the spatial patterns of carbon emissions and sequestration of Beijing from 2000 to 2020, the carbon metabolism processes between urban components were quantified, and the spatial pattern of urban carbon transitions caused by land use change was described. The results verified the harmful carbon transitions from the conversion of natural components to artificial components, which simultaneously brought a sharp decline in carbon sequestration and an increase in carbon emissions. The spatial pattern of urban carbon transitions indicated that the harmful carbon transitions always lay in and around the center of the southeast plain and some northwest mountainous districts, and the hotspot areas shifted outward over time. Beneficial carbon flows included the conversion of transportation and industrial land to urban land or rural land, bringing carbon emission reduction, and land use transfers out and into forest or grass, making carbon sequestration increase. The beneficial carbon flows were mainly distributed in the northwest mountainous region, which benefitted from "one-million-mu afforestation and greening project in plain areas" and were more widespread after 2010 than before. The overall carbon metabolism of the whole city was more beneficial in the latter decade than in the former decade. Specifically, this study also assessed the carbon metabolism of the unconverted land use type in addition to the carbon flows caused by the transformation of the land use type. The unconverted natural components embodied more beneficial carbon effects after 2010 since the carbon sequestration density significantly increased after 2010. The artificial components that remained unchanged showed a beneficial carbon effect after 2010, as the carbon emission density decreased while the carbon sequestration simultaneously increased.

These above findings provide important insights into the urban carbon metabolism of Beijing and quantitative evidence on which carbon flows and key areas can be primarily

targeted for adjustment to reduce carbon emissions or enhance carbon sequestration. This knowledge will help policymakers to focus on the primary aspects that provide the greatest benefit in launching locally targeted land use controls to develop a low-carbon city. Finally, continuing research work on improving the spatial and temporal resolution of urban carbon metabolism is warranted to detect the impact factors and the driving mechanism and simulate the urban carbon metabolism in different scenarios.

References

1. Mi, Z.; Guan, D.; Liu, Z.; Liu, J.; Viguié, V.; Fromer, N.; Wang, Y. Cities: The core of climate change mitigation. *J. Clean. Prod.* **2019**, *207*, 582–589. [CrossRef]
2. Song, X.P.; Hansen, M.C.; Stehman, S.V.; Potapov, P.V.; Tyukavina, A.; Vermote, E.F.; Townshend, J.R. Global land change from 1982 to 2016. *Nature* **2018**, *560*, 639–643. [CrossRef]
3. Fong, W.K.; Sotos, M.; Doust, M.; Schultz, S.; Marques, A.; Deng-Beck, C. *Global Protocol for Community-Scale Greenhouse Gas Inventories: An Accounting and Reporting Standard for Cities, Version 1.1*; Greenhouse Gas Protocoll: Washington, DC, USA, 2021.
4. IPCC. *Climate Change and Land: An IPCC Special Report on Climate Change, Desertification, Land Degradation, Sustainable Land Management, Food Security, and Greenhouse Gas Fluxes in Terrestrial Ecosystems*; Cambridge University Press: Cambridge, UK, 2019.
5. Zhu, Q.; Zeng, M.; Jia, P.; Guo, M.; Liang, X.; Guan, Q. Measuring the urban sprawl based on economic-dominated perspective: The case of 31 municipalities and provincial capitals. *Geo-Spat. Inf. Sci.* **2023**, 1–18. [CrossRef]
6. IPCC. *Climate Change 2022: Mitigation of Climate Change. Contribution of Working Group III to the Fifth Assessment Report of the Intergovernmental Panel on Climate Change*; Cambridge University Press: Cambridge, UK, 2022; pp. 923–1000.
7. Hong, C.; Burney, J.A.; Pongratz, J.; Nabel, J.E.M.S.; Mueller, N.D.; Jackson, R.B.; Davis, S.J. Global and regional drivers of land-use emissions in 1961–2017. *Nature* **2021**, *589*, 554–561. [CrossRef] [PubMed]
8. Lai, L.; Huang, X.; Yang, H.; Chuai, X.; Zhang, M.; Zhong, T.; Chen, Z.; Chen, Y.; Wang, X.; Thompson, J.R. Carbon emissions from land-use change and management in China between 1990 and 2010. *Sci. Adv.* **2016**, *2*, e1601063. [CrossRef] [PubMed]
9. Piao, S.; He, Y.; Wang, X.; Chen, F. Estimation of China's terrestrial ecosystem carbon sink: Methods, progress and prospects. *Sci. China Earth Sci.* **2022**, *65*, 641–651. [CrossRef]
10. Xu, J.; Wang, J.; Li, R.; Yang, X. Spatio-temporal effects of urbanization on CO_2 emissions: Evidences from 268 Chinese cities. *Energy Policy* **2023**, *177*, 113569. [CrossRef]
11. Chen, Q.; Su, M.; Meng, F.; Liu, Y.; Cai, Y.; Zhou, Y.; Yang, Z. Analysis of urban carbon metabolism characteristics based on provincial input-output tables. *J. Environ. Manag.* **2020**, *265*, 110561. [CrossRef]
12. Chen, S.; Long, H.; Chen, B. Assessing urban low-carbon performance from a metabolic perspective. *Sci. China Earth Sci.* **2021**, *64*, 1721–1734. [CrossRef]
13. Carpio, A.; Ponce-Lopez, R.; Lozano-Garcia, D.F. Urban form, land use, and cover change and their impact on carbon emissions in the Monterrey Metropolitan area, Mexico. *Urban Clim.* **2021**, *39*, 100947. [CrossRef]
14. Kang, T.; Wang, H.; He, Z.; Liu, Z.; Ren, Y.; Zhao, P. The effects of urban land use on energy-related CO_2 emissions in China. *Sci. Total Environ.* **2023**, *870*, 161873. [CrossRef] [PubMed]

15. Ren, Z.; Zheng, H.; He, X.; Zhang, D.; Shen, G.; Zhai, C. Changes in spatio-temporal patterns of urban forest and its above-ground carbon storage: Implication for urban CO_2 emissions mitigation under China's rapid urban expansion and greening. *Environ. Int.* **2019**, *129*, 438–450. [CrossRef] [PubMed]

16. He, Y.; Xia, C.; Shao, Z.; Zhao, J. The Spatiotemporal Evolution and Prediction of Carbon Storage: A Case Study of Urban Agglomeration in China's Beijing-Tianjin-Hebei Region. *Land* **2022**, *11*, 858. [CrossRef]

17. Liu, Q.; Yang, D.; Cao, L.; Anderson, B. Assessment and Prediction of Carbon Storage Based on Land Use/Land Cover Dynamics in the Tropics: A Case Study of Hainan Island, China. *Land* **2022**, *11*, 244. [CrossRef]

18. Wang, Z.; Li, X.; Mao, Y.; Li, L.; Wang, X.; Lin, Q. Dynamic simulation of land use change and assessment of carbon storage based on climate change scenarios at the city level: A case study of Bortala, China. *Ecol. Indic.* **2022**, *134*, 108499. [CrossRef]

19. Zheng, J.; Sun, N.; Yan, J.; Liu, C.; Yin, S. Decoupling between carbon source and sink induced by responses of daily stem growth to water availability in subtropical urban forests. *Sci. Total Environ.* **2023**, *877*, 162802. [CrossRef]

20. Namahoro, J.P.; Wu, Q.; Xiao, H.; Zhou, N. The Impact of Renewable Energy, Economic and Population Growth on CO_2 Emissions in the East African Region: Evidence from Common Correlated Effect Means Group and Asymmetric Analysis. *Energies* **2021**, *14*, 312. [CrossRef]

21. Zhu, B.; Shan, H. Impacts of industrial structures reconstructing on carbon emission and energy consumption: A case of Beijing. *J. Clean. Prod.* **2019**, *245*, 118916. [CrossRef]

22. Wang, Q.; Wang, L. The nonlinear effect of population aging, industrial structure, and urbanization on carbon emissions: A panel threshold regression analysis of 137 countries. *J. Clean. Prod.* **2020**, *287*, 125381. [CrossRef]

23. Han, L.; Xu, X.; Han, L. Applying quantile regression and Shapley decomposition to analyzing the determinants of household embedded carbon emissions: Evidence from urban China. *J. Clean. Prod.* **2015**, *103*, 219–230. [CrossRef]

24. Li, S.; Zhou, C. What are the impacts of demographic structure on CO_2 emissions? A regional analysis in China via heterogeneous panel estimates. *Sci. Total Environ.* **2018**, *650*, 2021–2031. [CrossRef] [PubMed]

25. Pottier, A. Expenditure-elasticity and income-elasticity of GHG emissions: A survey of literature on household carbon footprint. *Ecol. Econ.* **2022**, *192*, 107251. [CrossRef]

26. Zhao, R.Q.; Liu, Y.; Tian, M.M.; Ding, M.L.; Cao, L.H.; Zhang, Z.P.; Chuai, X.W.; Xiao, L.G.; Yao, L.G. Impacts of water and land resources exploitation on agricultural carbon emissions: The water-land-energy-carbon nexus. *Land Use Policy* **2018**, *72*, 480–492. [CrossRef]

27. Zhang, L.; Lin, X.; Xiao, Y.; Lin, Z. Spatial and structural characteristics of the ecological network of carbon metabolism of cultivated land based on land use and cover change: A case study of Nanchang, China. *Environ. Sci. Pollut. Res.* **2023**, *30*, 30514–30529. [CrossRef]

28. Cui, X.Z.; Li, S.Y.; Gao, F. Examining spatial carbon metabolism: Features, future simulation, and land-based mitigation. *Ecol. Model.* **2020**, *438*, 109325. [CrossRef]

29. Pianegonda, A.; Favargiotti, S.; Ciolli, M. Rural-Urban Metabolism: A Methodological Approach for Carbon-Positive and Circular Territories. *Sustainability* **2022**, *14*, 13964. [CrossRef]

30. Hutyra, L.R.; Yoon, B.; Hepinstall-Cymerman, J.; Alberti, M. Carbon consequences of land cover change and expansion of urban lands: A case study in the Seattle metropolitan region. *Landsc. Urban Plan.* **2011**, *103*, 83–93. [CrossRef]

31. Li, Y.; Shen, J.; Xia, C.; Xiang, M.; Cao, Y.; Yang, J. The impact of urban scale on carbon metabolism—A case study of Hangzhou, China. *J. Clean. Prod.* **2021**, *292*, 126055. [CrossRef]

32. Falahatkar, S.; Rezaei, F. Towards low carbon cities: Spatio-temporal dynamics of urban form and carbon dioxide emissions. *Remote Sens. Appl.-Soc. Environ.* **2020**, *18*, 100317. [CrossRef]

33. Xia, C.; Xiang, M.; Fang, K.; Li, Y.; Ye, Y.; Shi, Z.; Liu, J. Spatial-temporal distribution of carbon emissions by daily travel and its response to urban form: A case study of Hangzhou, China. *J. Clean. Prod.* **2020**, *257*, 120797. [CrossRef]

34. Liang, X.; Guan, Q.; Clarke, K.C.; Liu, S.; Wang, B.; Yao, Y. Understanding the drivers of sustainable land expansion using a patch-generating land use simulation (PLUS) model: A case study in Wuhan, China. *Comput. Environ. Urban Syst.* **2021**, *85*, 101569. [CrossRef]

35. Chuai, X.; Huang, X.; Lai, L.; Wang, W.; Peng, J.; Zhao, R. Land use structure optimization based on carbon storage in several regional terrestrial ecosystems across China. *Environ. Sci. Policy* **2013**, *25*, 50–61. [CrossRef]

36. Wang, J.; Feng, L.; Palmer, P.I.; Liu, Y.; Fang, S.; Bösch, H.; O'Dell, C.W.; Tang, X.; Yang, D.; Liu, L.; et al. Large Chinese land carbon sink estimated from atmospheric carbon dioxide data. *Nature* **2020**, *586*, 720–723. [CrossRef] [PubMed]

37. Qu, Y.; Zhang, J.; Xu, C.; Gao, Y.; Zheng, S.; Xia, M. Analysis of Spatial Carbon Metabolism by ENA: A Case Study of Tongzhou District, Beijing. *Land* **2022**, *11*, 1573. [CrossRef]

38. Xia, L.L.; Zhang, Y.; Yu, X.Y.; Fu, C.L.; Li, Y.G. An integrated analysis of input and output flows in an urban carbon metabolism using a spatially explicit network model. *J. Clean. Prod.* **2019**, *239*, 118063. [CrossRef]

39. Elliot, T.; Rugani, B.; Almenar, J.B.; Niza, S. A Proposal to Integrate System Dynamics and Carbon Metabolism for Urban Planning. In Proceedings of the 25th CIRP Conference on Life Cycle Engineering in Copenhagen, Copenhagen, Denmark, 30 April–2 May 2018.

40. Zhang, Y.; Linlin, X.; Weining, X. Analyzing spatial patterns of urban carbon metabolism: A case study in Beijing, China. *Landsc. Urban Plan.* **2014**, *130*, 184–200. [CrossRef]

41. Xia, C.Y.; Li, Y.; Xu, T.B.; Ye, Y.M.; Shi, Z.; Peng, Y.; Liu, J.M. Quantifying the spatial patterns of urban carbon metabolism: A case study of Hangzhou, China. *Ecol. Indic.* **2018**, *95*, 474–484. [CrossRef]
42. Wei, J.; Xia, L.; Chen, L.; Zhang, Y.; Yang, Z. A network-based framework for characterizing urban carbon metabolism associated with land use changes: A case of Beijing city, China. *J. Clean. Prod.* **2022**, *371*, 133695. [CrossRef]
43. Zhuang, Q.; Shao, Z.; Li, D.; Huang, X.; Li, Y.; Altan, O.; Wu, S. Impact of global urban expansion on the terrestrial vegetation carbon sequestration capacity. *Sci. Total Environ.* **2023**, *879*, 163074. [CrossRef]
44. Yin, L.; Sharifi, A.; Liqiao, H.; Jinyu, C. Urban carbon accounting: An overview. *Urban Clim.* **2022**, *44*, 101195. [CrossRef]
45. Potter, C.S.; Randerson, J.T.; Field, C.B.; Matson, P.A.; Vitousek, P.M.; Mooney, H.A.; Klooster, S.A. Terrestrial ecosystem production: A process model based on global satellite and surface data. *Glob. Biogeochem. Cycles* **1993**, *7*, 811–841. [CrossRef]
46. Zhu, W.; Pan, Y.; Zhang, J. Estimation of net primary productivity of Chinese terrestrial vegetation based on remote sensing. *Chin. J. Plant Ecol.* **2007**, *31*, 413–424. (In Chinese)
47. Huang, X.; He, L.; He, Z.; Nan, X.; Lyu, P.; Ye, H. An improved Carnegie-Ames-Stanford Approach model for estimating ecological carbon sequestration in mountain vegetation. *Front. Ecol. Evol.* **2022**, *10*, 1048607. [CrossRef]
48. Beijing Municipal Bureau of Statistics. *Beijing Statistical Yearbook*; China Statistics Press: Beijing, China, 2021. (In Chinese)
49. Resource and Environment Science and Data Center, China Land Use Remote Sensing Monitoring Dataset (CNLUCC). Available online: https://www.resdc.cn/DOI/DOI.aspx?DOIID=54 (accessed on 11 June 2020).
50. Liu, J.; Zhang, Z.; Xu, X.; Kuang, W.; Zhou, W.; Zhang, S.; Li, R.; Yan, C.; Yu, D.; Wu, S.; et al. Spatial patterns and driving forces of land use change in China during the early 21st century. *J. Geogr. Sci.* **2010**, *20*, 483–494. [CrossRef]
51. Liu, J.; Kuang, W.; Zhang, Z.; Xu, X.; Qin, Y.; Ning, J.; Zhou, W.; Zhang, S.; Li, R.; Yan, C.; et al. Spatiotemporal characteristics, patterns, and causes of land-use changes in China since the late 1980s. *J. Geogr. Sci.* **2014**, *24*, 195–210. [CrossRef]
52. Liang, X.; Liu, Z.; Zhai, L.; Ji, L.; Feng, Y.; Sang, H. Spatial terrestrial carbon emissions/sequestrations evolution based on ecological network analysis in Beijing-Tianjin-Hebei urban agglomeration. *Ecol. Eng.* **2023**, *189*, 106914. [CrossRef]
53. Didan, K. MOD13Q1 MODIS/Terra Vegetation Indices 16-Day L3 Global 250m SIN Grid V006. NASA EOSDIS Land Processes DAAC. 2022. Available online: https://catalog.data.gov/dataset/modis-terra-vegetation-indices-16-day-l3-global-250m-sin-grid-v006 (accessed on 1 June 2023).
54. National Bureau of Statistics and Energy Bureau of National Development and Reform Commission. *China Energy Statistical Yearbook*; China Statistics Press: Beijing, China, 2021. (In Chinese)
55. Zhang, Y.; Xia, L.; Fath, B.D.; Yang, Z.; Yin, X.; Su, M.; Liu, G.; Li, Y. Development of a spatially explicit network model of urban metabolism and analysis of the distribution of ecological relationships: Case study of Beijing, China. *J. Clean. Prod.* **2016**, *112*, 4304–4317. [CrossRef]
56. Zhu, W.; Pan, Y.; He, H.; Yu, D.; Haibo, H. Simulation of maximum light use efficiency for some typical vegetation types in China. *Chin. Sci. Bull.* **2006**, *51*, 7. [CrossRef]
57. Song, M.; Zhao, Y.; Liang, J.; Li, F. Spatial-temporal variability of carbon emission and sequestration and coupling coordination degree in Beijing district territory. *Clean. Environ. Syst.* **2023**, *8*, 100102. [CrossRef]
58. Resource and Environment Science and Data Center, China Net Primary Production Dataset. Available online: https://www.resdc.cn/data.aspx?DATAID=204 (accessed on 6 July 2022).
59. Runing, S. MOD17A3 MODIS/Terra Net Primary Production Gap-Filled Yearly L4 Global 500m SIN Grid V061. NASA EOSDIS Land Processes DAAC. 2023. Available online: https://data.nasa.gov/dataset/MODIS-Terra-Net-Primary-Production-Gap-Filled-Year/4fyi-5pxq (accessed on 1 June 2023).
60. Xia, C.Y.; Li, Y.; Xu, T.B.; Chen, Q.X.; Ye, Y.M.; Shi, Z.; Liu, J.M.; Ding, Q.L.; Li, X.S. Analyzing spatial patterns of urban carbon metabolism and its response to change of urban size: A case of the Yangtze River Delta, China. *Ecol. Indic.* **2019**, *104*, 615–625. [CrossRef]
61. Local Accounting Standards of Carbon Dioxide Emission in Beijing. Available online: https://www.bjets.com.cn/article/zcfg/202205/20220500002186.shtml (accessed on 6 July 2022).
62. Kuang, Y.Q.; Ouyang, T.P.; Zou, Y.; Liu, Y.; Li, C.; Wang, D.H. Present situation of carbon source and sink and potential for increase of carbon sink in Guangdong Province. *China Popul. Resour. Environ.* **2010**, *2012*, 56–61.
63. Fang, J.Y.; Liu, G.H.; Xu, S.L. *Carbon Cycle of Terrestrial Ecosystem in China and Its Global Meaning*; China Environmental Science Press: Beijing, China, 1996. (In Chinese)